
SV2A PET Imaging Is a Noninvasive Marker for the Detection of Spinal Damage in Experimental Models of Spinal Cord Injury

Daniele Bertoglio¹, Nicolas Halloin², Stef De Lombaerde^{1,3}, Aleksandar Jankovski^{4,5}, Jeroen Verhaeghe¹, Charles Nicaise^{*2}, and Steven Staelens^{*1}

¹Molecular Imaging Center Antwerp, University of Antwerp, Antwerp, Belgium; ²URPhyM–NARILIS, University of Namur, Namur, Belgium; ³Department of Nuclear Medicine, Antwerp University Hospital, Antwerp, Belgium; ⁴Institute of NeuroScience, NEUR Division, Université Catholique de Louvain, Louvain, Belgium; and ⁵Department of Neurosurgery, CHU UCL Namur, Yvoir, Belgium

Traumatic spinal cord injury (SCI) is a neurologic condition characterized by long-term motor and sensory neurologic deficits as a consequence of an external physical impact damaging the spinal cord. Anatomic MRI is considered the gold-standard diagnostic tool to obtain structural information for the prognosis of acute SCI; however, it lacks functional objective information to assess SCI progression and recovery. In this study, we explored the use of synaptic vesicle glycoprotein 2A (SV2A) PET imaging to detect spinal cord lesions noninvasively after SCI.

Methods: Mice ($n = 7$) and rats ($n = 8$) subjected to unilateral moderate cervical (C5) contusion were euthanized 1 wk after SCI for histologic and autoradiographic (³H-labeled (4*R*)-1-[(3-methylpyridin-4-yl)methyl]-4-(3,4,5-trifluorophenyl)pyrrolidin-2-one [UCB-J]) investigation of SV2A levels. Longitudinal ¹¹C-UCB-J PET/CT imaging was performed in sham ($n = 7$) and SCI rats ($n = 8$) 1 wk and 6 wk after SCI. Animals also underwent an ¹⁸F-FDG PET scan during the latter time point. Postmortem tissue SV2A analysis to corroborate in vivo PET findings was performed 6 wk after SCI. **Results:** A significant SV2A loss (ranging from -70.3% to -87.3% ; $P < 0.0001$) was measured at the epicenter of the impact in vitro in both mouse and rat contusion SCI models. Longitudinal ¹¹C-UCB-J PET imaging detected SV2A loss in SCI rats ($-49.0\% \pm 8.1\%$ at 1 wk and $-52.0\% \pm 12.9\%$ at 6 wk after SCI), with no change observed in sham rats. In contrast, ¹⁸F-FDG PET imaging measured only subtle hypometabolism ($-17.6\% \pm 14.7\%$). Finally, postmortem ³H-UCB-J autoradiography correlated with the in vivo SV2A PET findings ($r = 0.92$, $P < 0.0001$). **Conclusion:** ¹¹C-UCB-J PET/CT imaging is a noninvasive marker for SV2A loss after SCI. Collectively, these findings indicate that SV2A PET may provide an objective measure of SCI and thus represent a valuable tool to evaluate novel therapeutics. Clinical assessment of SCI with SV2A PET imaging is highly recommended.

Key Words: SV2A; ¹¹C-UCB-J; biomarker; contusion SCI; animal model

J Nucl Med 2022; 63:1245–1251
DOI: 10.2967/jnumed.121.263222

Spinal cord injury (SCI) is a devastating condition characterized by long-term motor and sensory neurologic deficits as well as a strong impact on the cognitive and social life of patients (1). Traumatic SCI is the consequence of an external physical impact damaging the spinal cord, with the neurologic outcomes being related to the extent of the primary lesion (1,2).

Currently, MRI is considered the gold-standard diagnostic tool to obtain structural information on spinal cord lesions and neighboring tissues during the acute phase of SCI (3–5). Although offering a clear view of the cord edema, hemorrhage, or syrinx formation, routine 1.5-T MRI has been shown to inconsistently correlate with the neurologic findings (6–8). Since MRI-based prognostication, treatment, and rehabilitation planning for spinally injured patients remain a daily clinical challenge (9), there has been increasing interest in developing objective imaging modalities to assess SCI progression and recovery for the noninvasive assessment of emerging therapeutic approaches (4–6).

PET imaging of glucose metabolism using ¹⁸F-FDG may represent an imaging modality to monitor metabolic activation and functional neuronal viability at the trauma epicenter. ¹⁸F-FDG PET imaging has been performed on both animal models and SCI patients, demonstrating abnormal metabolic activity in animals during the acute phase of experimental SCI or in patients during the active phases of compressive myelopathies (10–15). Although useful, the significance of the ¹⁸F-FDG signal remains flawed by its unspecific nature, mixing neuronal metabolism and glial activation (16), and by the lack of correlation with neurologic functions (17).

Recently, novel radioligands based on the antiepileptic drug levetiracetam and targeting the synaptic vesicle glycoprotein 2A (SV2A), a presynaptic protein regulating neurotransmitter release (18), have been developed (19). These ligands, including the selective and high-affinity radioligand ¹¹C-labeled (4*R*)-1-[(3-methylpyridin-4-yl)methyl]-4-(3,4,5-trifluorophenyl)pyrrolidin-2-one (UCB-J), have emerged as powerful tools to quantify synaptic density in vivo noninvasively (20,21). SV2A PET imaging has already proven a useful tool for assessing synaptic density in various neurodegenerative and neuropsychiatric disorders at clinical and preclinical stages (22–24).

Although SV2A PET imaging has been applied mainly to the brain, SV2A is also present in the gray matter of the spinal cord (25). Furthermore, we recently showed that ¹¹C-UCB-J PET imaging can quantify SV2A density noninvasively in the rodent spinal cord (23). We therefore postulated that SV2A PET imaging could serve as a

Received Sep. 14, 2021; revision accepted Nov. 30, 2021.

For correspondence or reprints, contact Steven Staelens (steven.staelens@uantwerpen.be).

*Contributed equally to this work.

Published online Jan. 13, 2022.

Immediate Open Access: Creative Commons Attribution 4.0 International License (CC BY) allows users to share and adapt with attribution, excluding materials credited to previous publications. License: <https://creativecommons.org/licenses/by/4.0/>. Details: <http://jnm.snmjournals.org/site/misc/permission.xhtml>.

COPYRIGHT © 2022 by the Society of Nuclear Medicine and Molecular Imaging.

biomarker of synaptic loss after SCI. In this study, we explored SV2A levels in experimental models of cervical contusion (26,27), investigated the potential of noninvasive ^{11}C -UCB-J PET imaging to detect spinal damage in rats after SCI, and compared ^{11}C -UCB-J and ^{18}F -FDG PET imaging to verify whether SV2A PET could provide enhanced specificity and sensitivity in detecting spinal injury.

MATERIALS AND METHODS

Animals and Experimental Design

All experiments complied with the European Communities Council Directive (2010/63/EU) and were authorized by the local animal ethic committees (University of Namur [UN19-339] and University of Antwerp [ECD2019-49]). Experiment outcomes were determined at 1 wk after SCI (subacute phase) and 6 wk after SCI (chronic phase), as outlined in Supplemental Figure 1 (supplemental materials are available at <http://jnm.snmjournals.org>). First, we investigated in vitro both mouse and rat models to assess whether SV2A levels were affected differentially between species. For the longitudinal in vivo study, the rat model was preferred given its favorable body and spinal cord size compared with mice. Nonetheless, investigation in mice is relevant given the abundance of genetic mouse models with relevant spinal cord diseases (23,28).

Adult male C57BL/6J mice ($n = 7$; body weight, 20–25 g) (internally bred at the University of Namur) and female Sprague–Dawley rats ($n = 8$; body weight, 225–275 g) (Charles River Laboratories) underwent SCI and were euthanized 1 wk after SCI for histologic and autoradiographic assessment of SV2A. An additional 15 female Sprague–Dawley rats (225–275 g) were subjected either to SCI ($n = 8$) or laminectomy only (sham, $n = 7$) and were included in the longitudinal PET study and euthanized at 6 wk after SCI. The animals were group-housed under a 12-h light/dark cycle in a temperature- and humidity-controlled environment with food and water ad libitum.

Contusion SCI

The animals underwent a cervical C5 unilateral right-sided contusion as previously described for mice (26) and rats (27). The animals were anesthetized using a mix of ketamine, 100 mg/kg (ketamine 1000; Ceva), and xylazine, 5 mg/kg (XYL-M 2%; VMD). Briefly, dorsal skin and underlying muscles were cut to access the spine between the spinous processes C2 and T1. The paravertebral muscles overlying C3–C5 were carefully removed. The animals were then subjected to laminectomy at the C5 vertebra before receiving a computer-controlled impact of 51.3 ± 1.7 kdynes for mice and 407 ± 6.1 kdynes for rats (dwell time of 0 s) using an IH Spinal Cord Impactor (Precision Systems and Instrumentation, LLC). The full procedure included unilateral laminectomy on the right side, clamping of the spinous processes of C2 and T2 using toothed Adson forceps to stabilize the whole spinal column, raising of the impactor tip (1.0-mm-diameter impactor for mice and 1.5 mm for rats) 2.5 mm above the dura, and contusion of the right hemicord (bathed in 0.9% sterile saline for rats). Muscles were sutured in layers using silk 2.0 (mice) or 4.0 (rats), and the skin was closed using surgical clippers. The animals received buprenorphine subcutaneously (Vetergesic; Ceva) at a dose of 0.05 mg/kg for analgesia after surgery and again 12 and 24 h after surgery. Saline was subcutaneously administered for rehydration immediately after surgery and 24 h later. One SCI rat did not recover from the surgical procedure and was euthanized. Sham animals underwent the full laminectomy procedure without contusion.

Radiosynthesis

^{11}C -UCB-J synthesis was performed on an automated synthesis module (Carbosynthon I; Comecer) as previously described (20,23), with an

average molar activity of 52.9 ± 12.4 GBq/ μmol . Radiochemical purity was greater than 99% for both ^{11}C -UCB-J and ^{18}F -FDG. ^3H -UCB-J (Novandi Chemistry AB) was synthesized with a molar radioactivity of 2,997 MBq/ μmol and radiochemical purity of more than 99%.

Small-Animal PET Imaging

Small-animal PET/CT was performed on 2 Siemens Inveon PET/CT scanners (Siemens Preclinical Solutions). The animals were prepared as previously described (29). For the ^{18}F -FDG PET scan, the animals were kept fasting starting the evening before the scan, for an average of 17.7 ± 1.6 h. Glucose strips (OneTouch Ultra 2; LifeScan) were used to measure the glucose concentration (81.2 ± 15.1 mg/dL) in duplicate from blood samples obtained via the tail vein of the rats before radioligand injection. The rats were anesthetized using isoflurane (Forane; Ohio Medical Products) in medical oxygen (induction, 5%; maintenance, 2%–2.5%). The respiration rate and body temperature were monitored and kept constant during the scan. ^{11}C -UCB-J PET images were acquired dynamically (50-min scan), whereas static (20-min) ^{18}F -FDG PET scans were obtained for glucose metabolism after 30 min of radioligand uptake in animals that were awake (29,30). Into a catheterized tail vein over a 30-s interval (1 mL/min) using an automated pump (Pump 11 Elite; Harvard Apparatus), a bolus of ^{11}C -UCB-J (6.7 ± 4.0 MBq) or ^{18}F -FDG (25.1 ± 2.0 MBq) was injected. Data were acquired in list-mode format. After the small-animal PET scan, a 10-min 80 kV/500 μA CT scan was performed for coregistration and attenuation correction.

Image Processing and Analysis

^{11}C -UCB-J data were reconstructed into 31 frames of increasing length (12×10 s, 3×20 s, 3×30 s, 3×60 s, 3×150 s, and 7×300 s), whereas a static reconstruction was applied to ^{18}F -FDG data using 8 iterations and 16 subsets of the 3-dimensional ordered-subset expectation maximization algorithm with spatially variant modeling (31) and normalization, dead-time, and CT-based attenuation corrections. Images were reconstructed on a $128 \times 128 \times 159$ grid with $0.776 \times 0.776 \times 0.796$ mm³ voxels. PET/CT images were processed and analyzed using PMOD software (version 3.6; PMOD Technologies).

To align all brains to a common space and use the same volume of interest to extract the whole-brain activity, brain PET images were rigid-matched to the Schiffer rat ^{18}F -FDG template (32) or the ^{11}C -UCB-J PET template (generated in the same space as the Schiffer one). Cervical spinal cord volumes of interest were manually delineated using the individual coregistered PET/CT images from C3 to C7, with C5 subdivided into right and left segments. Since we anticipated a potential partial-volume effect on the contralateral C5 segment, comparisons were made against the C3 section. The volumes of interest were kept at the same volume across subjects (0.016 cm³ at each C3–C7 level and 0.008 cm³ for left and right C5). Across animals, volumes of interest were manually reoriented to follow the profile of the spine. Supplemental Figure 2 shows the CT image of the spine in a representative sham rat with laminectomy.

For ^{11}C -UCB-J analysis, the interval from 25 to 45 min after injection was selected to determine radioligand uptake measured using SUV, calculated as brain activity multiplied by body weight and divided by the injected dose. No difference in cerebral uptake was observed for either ^{11}C -UCB-J (SUV) (Supplemental Fig. 3) or ^{18}F -FDG (SUV corrected for glucose levels) (Supplemental Fig. 4); therefore, spinal uptake was measured as the ratio of regional spinal uptake over whole-brain uptake.

Histologic Analysis

At 1 or 6 wk after injury, the animals were deeply anesthetized with sodium pentobarbital (50 mg/kg, intraperitoneally) and transcardially perfused with ice-cold phosphate-buffered saline (pH 7.4). The spinal

cords were dissected, and a cervical segment containing the contusion injury was snap-frozen in 2-methylbutane at -35°C for 2 min and preserved at -80°C until use. Coronal sections (30 μm thick) were collected on Superfrost Plus slides (Thermo Fischer Scientific) using a cryostat (Leica) and were distributed into a series of 12 slices so that each slide covered rostral, trauma, and caudal sections.

SV2A immunostaining was performed as previously described (23), using the primary antibody anti-SV2A (rabbit IgG; 1:400; catalog number 66724 [Cell Signaling Technologies]) followed by the secondary fluorescent antibody (donkey antirabbit; 1:100; Alexa Fluor 488 [Jackson ImmunoResearch]). Images were acquired at $\times 10$ magnification for quantification with a fluorescence microscope (Olympus) using CellSens software. Images were analyzed using Fiji (version 2.1.0) ImageJ software (National Institutes of Health). SV2A signal intensity was measured in regions of interest (right and left gray matter spinal cord) manually delineated on each section. Adjacent slides were stained with hematoxylin and eosin to visualize tissue morphology.

Autoradiography

In vitro ^3H -UCB-J (Novandi Chemistry AB) autoradiography was performed as previously reported (23). Mouse and rat SV2A selectivity in the spinal cord was validated using a blocking solution (1 nM of ^3H -UCB-J plus 1 mM of levetiracetam in binding buffer) (Supplemental Fig. 5).

Regional quantification was performed using Fiji (version 2.1.0) ImageJ software. Specific binding of ^3H -UCB-J was measured by converting the mean gray values into radioactivity density (Bq/mg), calculated using commercial tritium standards (American Radiolabeled Chemicals). Next, from ^3H -UCB-J molar activity on the experimental day, radioactivity density was converted into binding density (pmol/mg) for each region.

Statistical Analysis

In vivo spinal cord PET data, as well as postmortem analyses, were investigated using 2-way ANOVA (experimental group and region as variables). A decrease in spinal PET signal compared with C3 and cerebral binding was assessed using the Mann–Whitney test. Autoradiographic blocking experiments were analyzed using paired t tests. Correlations between in vivo and postmortem SV2A signals were evaluated using a Spearman r test. P values were corrected for multiple comparisons using the Šídák multiple-comparisons test. Statistical analyses were performed with GraphPad Prism (version 9.1) statistical software. Data are represented as mean \pm SD. All tests were 2-tailed, and statistical significance was set at a P value of less than 0.05.

RESULTS

SV2A Levels Are Decreased Subacutely in Experimental Models of Contusion SCI

To determine whether SV2A levels are changed after a spinal injury, we performed SV2A histologic and autoradiographic assessment on 2 experimental models of contusion SCI during the subacute phase (Fig. 1A; Supplemental Fig. 6A). In both mouse and rat spinal cord, a significant SV2A loss at the epicenter of impact, but not in rostral sections (C3–C4 level), was observed with SV2A immunostaining (contralateral effect: mouse, $F_{1,24} = 140.4$ [$P < 0.0001$]; rat, $F_{1,28} = 20.2$ [$P < 0.0001$]), which corresponded to an approximately 80% decline compared with rostral sections (mouse, $-81.2\% \pm 8.6\%$ [post hoc $P < 0.0001$]; rat, $-78.8\% \pm 21.1\%$ [post hoc $P < 0.0001$]) (Fig. 1B; Supplemental Fig. 6B). Analogously, ^3H -UCB-J binding was significantly affected at the epicenter of the contusion compared with the contralateral side (contralateral effect: mouse, $F_{1,24} = 42.3$ [$P <$

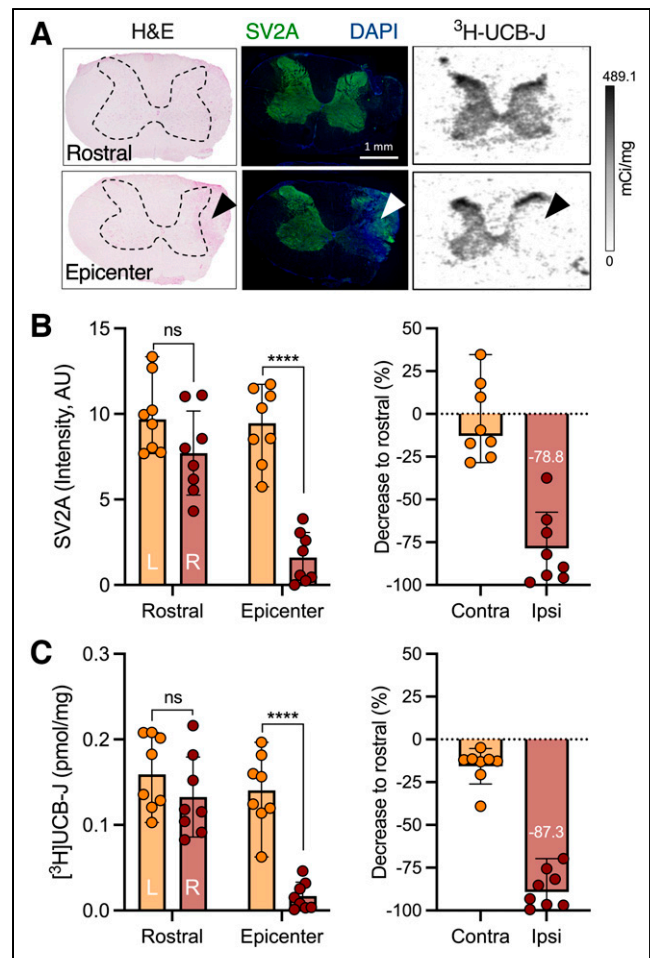


FIGURE 1. SV2A levels are decreased in rat model of contusion SCI. (A) Representative hematoxylin and eosin, SV2A, and ^3H -UCB-J images depicting rostral and epicenter spinal cord sections. Arrowheads indicate contusion site at right C5 vertebra; dashed lines outline spinal gray matter. (B and C) SV2A (B) and ^3H -UCB-J (C) quantification in spinal cord sections and decrease in C5 section compared with rostral for both contralateral (left) and ipsilateral (right) sides. AU = arbitrary units; H&E = hematoxylin and eosin; ns = not statistically significant. **** $P < 0.0001$.

0.0001]; rat, $F_{1,28} = 24.4$ [$P < 0.0001$]), with a clear decline in relation to rostral sections (mouse, $-70.3\% \pm 11.5\%$ [post hoc $P < 0.0001$]; rat, $-87.3\% \pm 10.9\%$ [post hoc $P < 0.0001$]) (Fig. 1C; Supplemental Fig. 6C). Notably, the SV2A loss was not due to loss of spinal tissue, as depicted by the hematoxylin and eosin staining.

^{11}C -UCB-J PET Detects In Vivo SV2A Loss After SCI

Given the wider diameter of the spinal cord in the rat, the rat model was chosen to investigate ^{11}C -UCB-J PET imaging after SCI. Figure 2 displays representative ^{11}C -UCB-J uptake images in a SCI rat compared with a sham control rat 1 wk after injury. Spinal cord ^{11}C -UCB-J uptake at the contusion site (right C5) was significantly changed compared with sham animals (group effect, $F_{1,54} = 100.2$ [$P < 0.0001$]) (Fig. 3A). ^{11}C -UCB-J uptake was also significantly reduced in surrounding areas (C4, left C5, and C6). Accordingly, SCI animals displayed a ^{11}C -UCB-J binding decline in right C5 compared with C3 ($-49.0\% \pm 8.1\%$), which significantly differed from sham rats ($P = 0.0043$) (Fig. 3B).

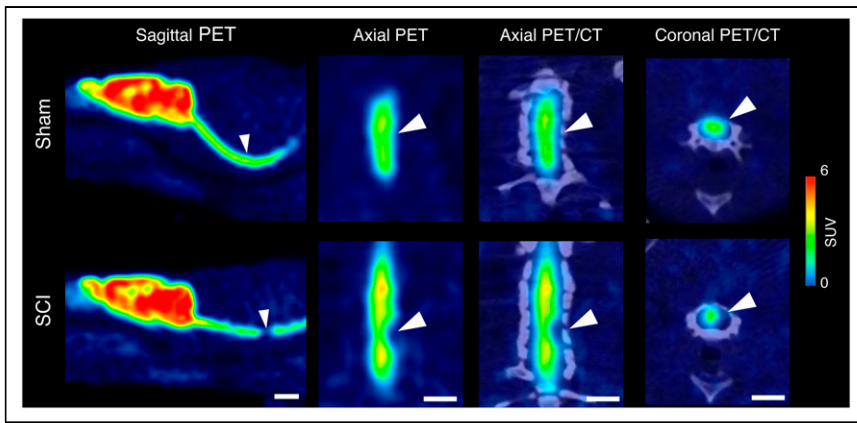


FIGURE 2. Representative ^{11}C -UCB-J PET images are shown of sham and SCI rat 1 wk after trauma. Arrowheads indicate contusion site at C5 vertebra. Interval is 25–45 min after injection. Scale bar = 5 mm.

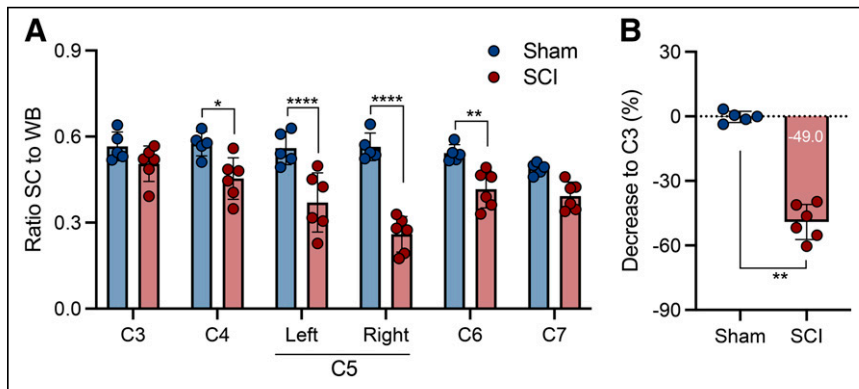


FIGURE 3. ^{11}C -UCB-J PET detects SV2A loss in contusion SCI rat model. (A) Significant reduction in spinal cord ^{11}C -UCB-J uptake around contusion site (right C5), compared with sham animals. (B) Spinal cord ^{11}C -UCB-J uptake at epicenter (right C5) compared with C3 level within each animal. SC = spinal cord; WB = whole brain. * $P < 0.05$. ** $P < 0.01$. **** $P < 0.0001$.

^{11}C -UCB-J PET Outperforms ^{18}F -FDG PET for Detection of Chronic SCI

Similarly to 1 wk after injury, the reduction in ^{11}C -UCB-J uptake around the contusion site (right C5) in SCI rats was significant and sustained at 6 wk after injury compared with sham animals (group effect, $F_{1,60} = 190.4$ [$P < 0.0001$]) (Fig. 4A). Hence, SCI animals displayed a ^{11}C -UCB-J binding decline in right C5 compared with C3 ($-52.0\% \pm 12.9\%$), which significantly differed from sham rats ($P = 0.0025$) (Fig. 4B). Interestingly, ^{11}C -UCB-J uptake at the site of chronic trauma in SCI rats was significantly affected until C7 ($P < 0.01$), unlike at 1 wk after SCI ($P > 0.05$), suggesting that the local contusion might induce SV2A loss caudal to the lesion epicenter.

Six weeks after SCI, the animals underwent ^{11}C -UCB-J and ^{18}F -FDG PET to assess whether SV2A PET could provide enhanced sensitivity in detecting spinal injury. ^{18}F -FDG PET could detect hypometabolism at the contusion epicenter (right C5) compared with sham animals (group effect, $F_{1,60} = 70.9$ [$P < 0.0001$]) (Fig. 5A), as well as hypometabolism in surrounding tissue (left C5 and C6). However, the difference compared with C3 was subtle ($-17.6\% \pm 14.7\%$), with no significant change from sham rats ($P = 0.106$) (Fig. 5B).

Postmortem Analysis Corroborates ^{11}C -UCB-J PET Findings

Similar to the analyses at the subacute phase, a significant SV2A loss at the epicenter, but not in rostral (C3 and C4) sections, was observed at the chronic phase with

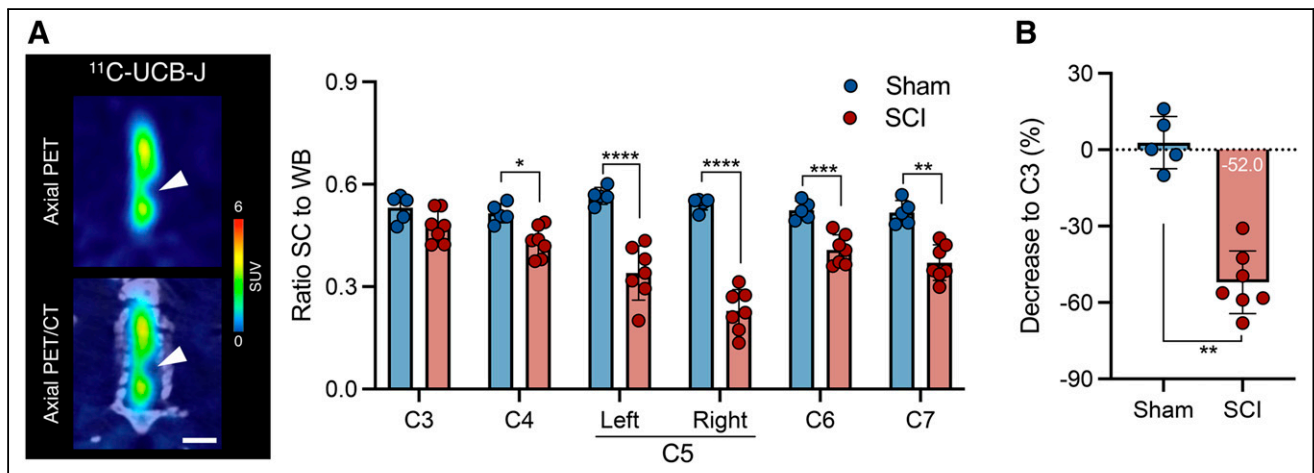


FIGURE 4. ^{11}C -UCB-J reduction is sustained during chronic SCI in contusion rat model. (A) Representative PET image of SCI rat and ^{11}C -UCB-J PET analysis of sham animals and rats with chronic SCI. Interval is 25–45 min after injection. Scale bar = 5 mm. (B) Spinal cord ^{11}C -UCB-J uptake at epicenter compared with C3 level within each animal. SC = spinal cord; WB = whole brain. * $P < 0.05$. ** $P < 0.01$. *** $P < 0.001$. **** $P < 0.0001$.

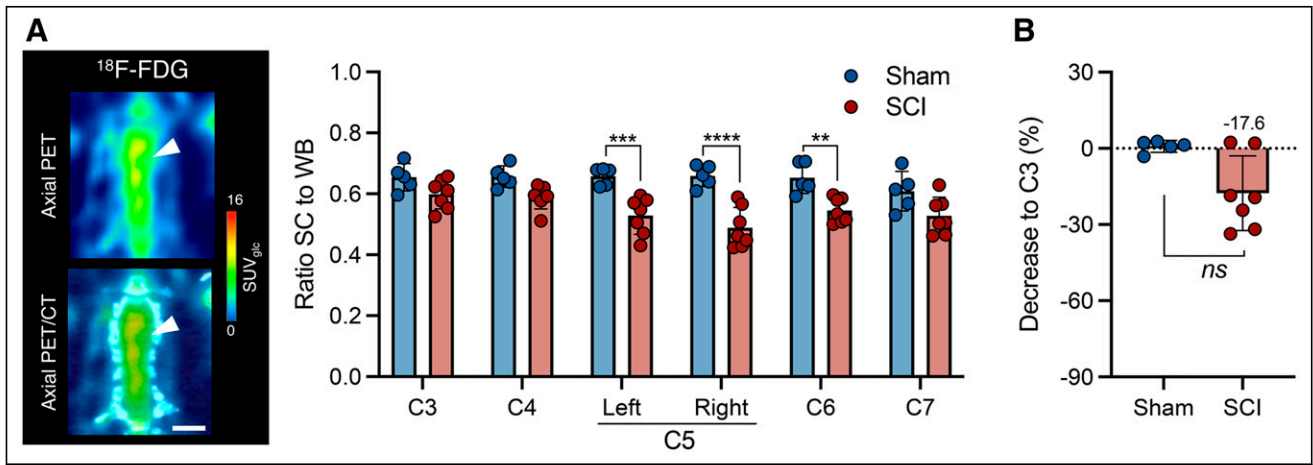


FIGURE 5. ^{18}F -FDG reduction is limited during chronic SCI in contusion rat model. (A) Representative PET image of SCI rat and ^{18}F -FDG PET analysis of sham animals and rats with chronic SCI. Scale bar = 5 mm. (B) Spinal cord ^{18}F -FDG uptake at epicenter compared with C3 level within each animal. SC = spinal cord; WB = whole brain. $**P < 0.01$. $***P < 0.001$. $****P < 0.0001$.

SV2A immunostaining (group effect, $F_{1,22} = 62.0$ [$P < 0.0001$]), corresponding to an $86\% \pm 17.4\%$ decline compared with rostral sections (Fig. 6A), showing strong consistency with the in vivo ^{11}C -UCB-J PET measurements ($r = 0.86$, $P = 0.0013$; Fig. 6B).

^3H -UCB-J binding was significantly affected as well (group effect, $F_{1,22} = 31.2$ [$P < 0.0001$]), with a $82.1\% \pm 22.8\%$ decline compared with rostral sections (Fig. 6C). ^3H -UCB-J autoradiography reflected the in vivo ^{11}C -UCB-J PET quantification ($r = 0.92$, $P < 0.0001$; Fig. 6D).

DISCUSSION

This study showed that SV2A is decreased in mouse and rat experimental models of SCI contusion and that synaptic loss after SCI can be measured noninvasively. Also, the SV2A decrease is sustained over time, and ^{11}C -UCB-J PET imaging provides a 3-fold enhanced sensitivity compared with ^{18}F -FDG PET imaging in assessing spinal damage. Collectively, these findings suggest that SV2A PET imaging could serve as a robust biomarker capable of detecting subtle synaptic loss after SCI.

Validation by histologic and autoradiographic findings confirmed that SV2A is restricted to gray matter (25) and that ^3H -UCB-J binding was blocked by levetiracetam (19). Both experimental models of SCI displayed a comparable unilateral SV2A loss; most importantly, the SV2A decline was not due to a mere tissue loss caused by the initial trauma.

For in vivo PET quantification, we focused on the comparison to the rostral C3 level (which is morphologically unaffected) to avoid the partial-volume effect that is likely present in the uninjured C5 hemicord. We measured a sustained reduction in ^{11}C -UCB-J binding at the SCI epicenter over time, suggesting little-to-no regeneration of synaptic connections and sprouting of spared axons. Notably, a decrease in SV2A was observed in SCI rats over time at the caudal level (C6 and C7). This decrease is a possible result of the deafferentation of the gray matter and consequent caudal synaptic loss, overall reflecting an extension of the secondary lesion, which comprises many processes: apoptosis, demyelination of surviving axons, axonal die-back, and building of a glial scar around the injury site (1,33,34).

Previous studies have reported only transient changes in ^{18}F -FDG uptake in rat and canine models (13,14). Thus, one objective of the current study was to compare the

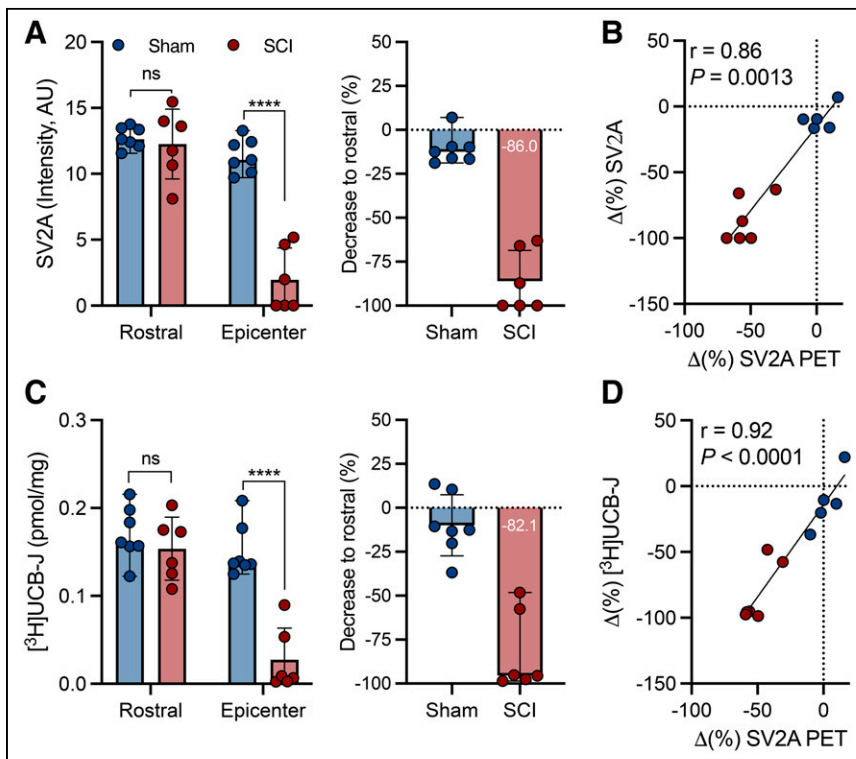


FIGURE 6. Postmortem analyses corroborated sustained SV2A loss measured with ^{11}C -UCB-J PET during chronic SCI. (A) SV2A immunofluorescence quantification. (B) Correlation between rostral and epicenter decrease measured with ^{11}C -UCB-J PET. (C) ^3H -UCB-J autoradiography quantification. (D) Correlation between rostral and epicenter decrease measured with ^{11}C -UCB-J PET. ns = not statistically significant. $****P < 0.0001$.

performance of ^{11}C -UCB-J with ^{18}F -FDG in detecting spinal cord damage. Despite the extensive neurodegeneration at the trauma site (1), the observed reduction in glucose uptake was only a fraction (-17.6%) compared with the SV2A loss (-52.0%). This is likely related to the enhanced gliosis driven by microglia/macrophage and astrocyte activation related to primary and secondary injuries. Since glucose uptake is the result of neuronal and glial metabolism (16), the gliosis occurring at the trauma site can largely mask the reduced uptake associated with neurodegeneration. As such, understanding the biologic process driving the ^{18}F -FDG uptake is challenging, especially for the assessment of therapeutics, because of the plethora of processes occurring at the injury site (1,34). In contrast, the precise nature of SV2A as the molecular target of ^{11}C -UCB-J offers a specific measure of synaptic density without being affected by secondary processes. Thus, SV2A PET imaging might provide a powerful tool for the assessment of synaptic loss in traumatic, neurodegenerative, inflammatory, and vascular spinal cord pathologies, as well as for synaptic loss, regeneration (24), and axonal connectivity after gene and cell therapy approaches (35). Future studies investigating the association between spinal SV2A density and degree of motor impairment will be needed to understand whether SV2A loss might represent a biomarker with functional relevance.

Despite being the gold-standard diagnostic tool to obtain structural information on spinal cord lesions during the acute phase of SCI (4), functional assessment based on MRI remains elusive, resulting in inconsistent correlations with the neurologic findings (6–8). Although novel approaches such as diffusion tensor imaging and myelin water transfer can provide added value in terms of axon and myelin integrity (4), their readouts are likely to be affected by evolving edema, hemorrhage, or syrinx formation. SV2A PET imaging can offer an attractive complementary alternative to objectively measure synaptic integrity at the lesion site in preclinical and clinical settings. Although we describe here for the first time (to our knowledge) spinal SV2A changes, SV2A PET imaging has already been performed in several clinical studies of neurologic disorders (22). With a more favorable resolution ratio (spinal cord/scanner resolution) available for human PET imaging, we foresee no limitation for clinical application, as supported by a preliminary report on healthy subjects (36). The high sensitivity of SV2A as compared with ^{18}F -FDG PET and the added value of ^{18}F -FDG PET as compared with MRI (15) suggest that SV2A PET may be of particular interest in the diagnosis and prognosis of cervical spondylotic myelopathy, which is common in the elderly (37).

CONCLUSION

Using ^{11}C -UCB-J PET/CT imaging, we successfully detected SV2A loss in the contusion SCI rat model. The presented findings indicate that synaptic loss after SCI can be quantified noninvasively, SV2A decrease is sustained over time, and ^{11}C -UCB-J PET imaging provides enhanced sensitivity compared with ^{18}F -FDG PET imaging for assessment of spinal damage. Collectively, these findings indicate that SV2A PET may provide an objective measure of SCI and thus be a valuable tool to evaluate novel therapeutics. Clinical assessment of SCI with SV2A PET imaging is highly recommended.

DISCLOSURE

Daniele Bertoglio is supported by the Research Foundation Flanders (FWO, 1229721N). Antwerp University also funded the work through a partial assistant professor position for Jeroen Verhaeghe

and a full professor position for Steven Staelens. Daniele Bertoglio, Jeroen Verhaeghe, and Steven Staelens are members of the μNeuro Research Centre of Excellence at the University of Antwerp. No other potential conflict of interest relevant to this article was reported.

ACKNOWLEDGMENTS

We thank Philippe Joye, Romy Raeymakers, and Annemie Van Eetveldt of MICA for their valuable technical assistance. Part of the graphical abstract and Supplemental Figure 1 were generated using BioRender.

KEY POINTS

QUESTION: Does SV2A represent a biomarker for SCI?

PERTINENT FINDINGS: SV2A levels are significantly reduced in animal models of contusion SCI. Longitudinal ^{11}C -UCB-J PET imaging showed that SV2A loss can be quantified noninvasively, is sustained over time, and outperforms ^{18}F -FDG PET imaging.

IMPLICATIONS FOR PATIENT CARE: SV2A PET imaging offers a novel noninvasive method to quantify SCI, which may provide a promising diagnostic tool for the assessment of functional recovery after SCI therapeutics.

REFERENCES

1. Ahuja CS, Wilson JR, Nori S, et al. Traumatic spinal cord injury. *Nat Rev Dis Primers*. 2017;3:17018.
2. Wilson JR, Hashimoto RE, Dettori JR, Fehlings MG. Spinal cord injury and quality of life: a systematic review of outcome measures. *Evid Based Spine Care J*. 2011;2:37–44.
3. Freund P, Curt A, Friston K, Thompson A. Tracking changes following spinal cord injury: insights from neuroimaging. *Neuroscientist*. 2013;19:116–128.
4. Freund P, Seif M, Weiskopf N, et al. MRI in traumatic spinal cord injury: from clinical assessment to neuroimaging biomarkers. *Lancet Neurol*. 2019;18:1123–1135.
5. Lammertse D, Dungan D, Dreisbach J, et al. Neuroimaging in traumatic spinal cord injury: an evidence-based review for clinical practice and research. *J Spinal Cord Med*. 2007;30:205–214.
6. Ellingson BM, Salamon N, Holly LT. Imaging techniques in spinal cord injury. *World Neurosurg*. 2014;82:1351–1358.
7. Chay W, Kirshblum S. Predicting outcomes after spinal cord injury. *Phys Med Rehabil Clin N Am*. 2020;31:331–343.
8. Sharif S, Jazaib Ali MY. Outcome prediction in spinal cord injury: myth or reality. *World Neurosurg*. 2020;140:574–590.
9. Talbott JF, Huie JR, Ferguson AR, Bresnahan JC, Beattie MS, Dhall SS. MR imaging for assessing injury severity and prognosis in acute traumatic spinal cord injury. *Radiol Clin North Am*. 2019;57:319–339.
10. Flanagan EP, Hunt CH, Lowe V, et al. [^{18}F]-fluorodeoxyglucose-positron emission tomography in patients with active myelopathy. *Mayo Clin Proc*. 2013;88:1204–1212.
11. Floeth FW, Stoffels G, Herdmann J, et al. Prognostic value of ^{18}F -FDG PET in monosegmental stenosis and myelopathy of the cervical spinal cord. *J Nucl Med*. 2011;52:1385–1391.
12. Nandoe Tewarie RD, Yu J, Seidel J, et al. Positron emission tomography for serial imaging of the contused adult rat spinal cord. *Mol Imaging*. 2010;9:108–116.
13. von Leden RE, Selwyn RG, Jaiswal S, Wilson CM, Khayrullina G, Byrnes KR. ^{18}F -FDG-PET imaging of rat spinal cord demonstrates altered glucose uptake acutely after contusion injury. *Neurosci Lett*. 2016;621:126–132.
14. Zhang L, López-Picón FR, Jia Y, et al. Longitudinal [^{18}F]FDG and [^{13}N]NH₃ PET/CT imaging of brain and spinal cord in a canine hemisection spinal cord injury model. *Neuroimage Clin*. 2021;31:102692.
15. Eicker SO, Langen KJ, Galldiks N, et al. Clinical value of 2-deoxy- [^{18}F]fluoro-D-glucose positron emission tomography in patients with cervical spondylotic myelopathy. *Neurosurg Focus*. 2013;35:E2.
16. Xiang X, Wind K, Wiedemann T, et al. Microglial activation states drive glucose uptake and FDG-PET alterations in neurodegenerative diseases. *Sci Transl Med*. 2021;13:eabe5640.

17. Byrnes KR, Wilson CM, Brabazon F, et al. FDG-PET imaging in mild traumatic brain injury: a critical review. *Front Neuroenergetics*. 2014;5:13.
18. Bajjalieh SM, Frantz GD, Weimann JM, McConnell SK, Scheller RH. Differential expression of synaptic vesicle protein 2 (SV2) isoforms. *J Neurosci*. 1994;14:5223–5235.
19. Lynch BA, Lambeng N, Nocka K, et al. The synaptic vesicle protein SV2A is the binding site for the antiepileptic drug levetiracetam. *Proc Natl Acad Sci USA*. 2004;101:9861–9866.
20. Bertoglio D, Verhaeghe J, Miranda A, et al. Validation and noninvasive kinetic modeling of [¹¹C]UCB-J PET imaging in mice. *J Cereb Blood Flow Metab*. 2020;40:1351–1362.
21. Finnema SJ, Nabulsi NB, Eid T, et al. Imaging synaptic density in the living human brain. *Sci Transl Med*. 2016;8:348ra96.
22. Cai Z, Li S, Matuskey D, Nabulsi N, Huang Y. PET imaging of synaptic density: a new tool for investigation of neuropsychiatric diseases. *Neurosci Lett*. 2019;691:44–50.
23. Bertoglio D, Verhaeghe J, Wyffels L, et al. Synaptic vesicle glycoprotein 2A is affected in the CNS of Huntington's disease mice and post-mortem human HD brain. *J Nucl Med*. September 16, 2021 [Epub ahead of print].
24. Toyonaga T, Smith LM, Finnema SJ, et al. In vivo synaptic density imaging with ¹¹C-UCB-J detects treatment effects of saracatinib in a mouse model of Alzheimer disease. *J Nucl Med*. 2019;60:1780–1786.
25. Lambeng N, Gillard M, Vertongen P, Fuks B, Chatelain P. Characterization of [³H]Jucb 30889 binding to synaptic vesicle protein 2A in the rat spinal cord. *Eur J Pharmacol*. 2005;520:70–76.
26. Nicaise C, Putatunda R, Hala TJ, et al. Degeneration of phrenic motor neurons induces long-term diaphragm deficits following mid-cervical spinal contusion in mice. *J Neurotrauma*. 2012;29:2748–2760.
27. Nicaise C, Hala TJ, Frank DM, et al. Phrenic motor neuron degeneration compromises phrenic axonal circuitry and diaphragm activity in a unilateral cervical contusion model of spinal cord injury. *Exp Neurol*. 2012;235:539–552.
28. Ross CA, Poirier MA. Protein aggregation and neurodegenerative disease. *Nat Med*. 2004;10(suppl):S10–S17.
29. Bertoglio D, Deleyme S, Miranda A, Stroobants S, Staelens S, Verhaeghe J. Estimation of the net influx rate K_i and the cerebral metabolic rate of glucose MRglc using a single static [¹⁸F]FDG PET scan in rats. *Neuroimage*. 2021;233:117961.
30. Deleyme S, Verhaeghe J, wyffels L, Dedeurwaerdere S, Stroobants S, Staelens S. Towards a reproducible protocol for repetitive and semi-quantitative rat brain imaging with ¹⁸F-FDG: exemplified in a memantine pharmacological challenge. *Neuroimage*. 2014;96:276–287.
31. Miranda A, Bertoglio D, Glorie D, Stroobants S, Staelens S, Verhaeghe J. Validation of a spatially variant resolution model for small animal brain PET studies. *Biomed Phys Eng Express*. 2020;6:045001.
32. Schiffer WK, Mirrione MM, Dewey SL. Optimizing experimental protocols for quantitative behavioral imaging with ¹⁸F-FDG in rodents. *J Nucl Med*. 2007;48:277–287.
33. Alizadeh A, Dyck SM, Karimi-Abdolrezaee S. Traumatic spinal cord injury: an overview of pathophysiology, models and acute injury mechanisms. *Front Neurol*. 2019;10:282.
34. Oyinbo CA. Secondary injury mechanisms in traumatic spinal cord injury: a nugget of this multiply cascade. *Acta Neurobiol Exp (Warsz)*. 2011;71:281–299.
35. Assinck P, Duncan GJ, Hilton BJ, Plemel JR, Tetzlaff W. Cell transplantation therapy for spinal cord injury. *Nat Neurosci*. 2017;20:637–647.
36. Rossano S, Bini J, Nabulsi N, Ropchan J, Carson RE. Feasibility of imaging synaptic density in the human spinal cord using ¹¹C-UCB-J PET [abstract]. *J Nucl Med*. 2021;61(suppl 1):112.
37. Kalsi-Ryan S, Karadimas SK, Fehlings MG. Cervical spondylotic myelopathy: the clinical phenomenon and the current pathobiology of an increasingly prevalent and devastating disorder. *Neuroscientist*. 2013;19:409–421.